Ocean Modelling 113 (2017) 22–29

Contents lists available at ScienceDirect

Ocean Modelling

journal homepage: www.elsevier.com/locate/ocemod

# The viscous lee wave problem and its implications for ocean modelling

Callum J. Shakespeare[a,b,*], Andrew McC. Hogg[a,b]

[a] Research School of Earth Sciences, Australian National University, Canberra, Australian Capital Territory
[b] Australian Research Council Centre of Excellence for Climate System Science, Australia

ARTICLE INFO

*Article history:*
Received 4 August 2016
Revised 5 March 2017
Accepted 7 March 2017
Available online 8 March 2017

*Keywords:*
Internal waves
Dissipation
Lee waves

ABSTRACT

Ocean circulation models employ 'turbulent' viscosity and diffusivity to represent unresolved subgridscale processes such as breaking internal waves. Computational power has now advanced sufficiently to permit regional ocean circulation models to be run at sufficiently high (100 m–1 km) horizontal resolution to resolve a significant part of the internal wave spectrum. Here we develop theory for boundary generated internal waves in such models, and in particular, where the waves dissipate their energy. We focus specifically on the steady lee wave problem where stationary waves are generated by a large-scale flow acting across ocean bottom topography. We generalise the energy flux expressions of [Bell, T., 1975. Topographically generated internal waves in the open ocean. J. Geophys. Res. 80, 320–327] to include the effect of arbitrary viscosity and diffusivity. Applying these results for realistic parameter choices we show that in the present generation of models with $\mathcal{O}(1)$ $m^2s^{-1}$ horizontal viscosity/diffusivity boundary-generated waves will inevitably dissipate the majority of their energy within a few hundred metres of the boundary. This dissipation is a direct consequence of the artificially high viscosity/diffusivity, which is not always physically justified in numerical models. Hence, caution is necessary in comparing model results to ocean observations. Our theory further predicts that $\mathcal{O}(10^{-2})$ $m^2s^{-1}$ horizontal and $\mathcal{O}(10^{-4})$ $m^2s^{-1}$ vertical viscosity/diffusivity is required to achieve a qualitatively inviscid representation of internal wave dynamics in ocean models.



## 1. Introduction

Internal waves are an important mechanism for vertical and downscale transfer of energy in the ocean. Internal waves can transport energy from the upper and lower boundary of the ocean (where much of the energy is injected) to the ocean interior, where wave breaking and other nonlinear processes can lead to turbulent mixing (Waterhouse et al., 2014). Furthermore, they are amongst the larger scales of 'unbalanced' flow, and can therefore provide a conduit from large-scale 'balanced' flow to the small-scale turbulence where dissipation occurs (Vanneste, 2013). Internal waves are generated by surface wind stresses (Alford et al., 2016; Jouanno et al., 2016), tidal interactions with bathymetry (e.g. St Laurent and Garrett, 2002), geostrophic flows over rough topography on the sea floor (Nikurashin and Ferrari, 2010), and small-scale unbalanced flow at the ocean surface including submesoscale eddies, fronts and filaments (e.g. Danioux et al., 2012; Nagai et al., 2015; Shakespeare and Taylor, 2016).

Only recently have computational capabilities expanded sufficiently to permit regional ocean circulation models to be run at sufficiently high (100 m–1 km) horizontal resolution to resolve a significant portion of the internal wave spectrum (Nikurashin et al., 2013; Nagai et al., 2015; Rosso et al., 2015). In their 200 m resolution model, Nikurashin et al. (2013) find that the resolved waves generated via geostrophic flow over topography (lee waves) dissipate 80% of their energy in the water column directly above the topography. They extrapolate this result to the global ocean to suggest that the resolved waves with scales exceeding 1 km provide a first-order contribution to turbulent mixing directly above topography, thereby sustaining the ocean overturning circulation. Enhanced dissipation above rough topography is consistent with ocean observations (Waterhouse et al., 2014). However, observational estimates suggest that lee waves only dissipate 2–20% of their energy near topography (Waterman et al., 2013), much less than the 80% predicted from the Nikurashin et al. (2013) numerical model.

As with all large-scale ocean models, the subgrid-scale turbulence in wave-resolving numerical models must be parameterised, typically using Laplacian (or higher order) horizontal diffusivities

* Corresponding author.
*E-mail address:* callum.shakespeare@anu.edu.au (C.J. Shakespeare).

http://dx.doi.org/10.1016/j.ocemod.2017.03.006
1463-5003/

and/or viscosities. The fact that the horizontal gridscale (100 m–1 km) is much larger than the vertical (1–20 m) implies that the corresponding viscosity/diffusivity will be that much larger: typical values of Laplacian horizontal diffusivities and/or viscosities employed in these high resolution models (e.g. Nikurashin et al., 2013; Nagai et al., 2015; Rosso et al., 2015) are of $\mathcal{O}(1)$ m$^2$ s$^{-1}$ throughout the depth of the ocean. In comparison, values for vertical viscosity/diffusivity are typically of $\mathcal{O}(10^{-3} - 10^{-5})$ m$^2$ s$^{-1}$. To some extent these parameterisations are intended to represent the effect of internal waves breaking and driving mixing of density and momentum in the ocean interior (Polzin, 2010; Polzin and Lvov, 2011). This situation presents a problem since we are parameterising the effect of waves while partially resolving waves, and thus any effect the parameterisation has on the waves is potentially a spurious one. Here we investigate this effect and what can be done to minimise or eliminate it. It it widely acknowledged that numerical ocean models should be run with the smallest possible turbulent viscosities and diffusivities[1], except in regions of the ocean where larger values can be physically justified. However, values considered 'small' change with model resolution as smaller-scale physics is explicitly represented— here we quantify what values are 'small enough' in the context of internal waves in wave-resolving models, and the constraint this places on model resolution.

The 'fluid' in the numerical models described above (which we will term the 'model fluid') has strongly non-isotropic behaviour, with order-of-magnitude different horizontal and vertical viscosity/diffusivity. As will be shown here, these parameter choices result in the energy loss from the wave field in large-scale numerical models often being dominated by the horizontal viscosity/diffusivity for much of the internal wave spectrum (excluding near-inertial waves). Most of these models also use the hydrostatic version of the Boussinesq equations, so we will only consider hydrostatic internal waves. Thus, our objective here is to formulate hydrostatic linear internal wave theory to describe the energy flux associated with boundary-sourced internal waves in the presence of arbitrary viscosity/diffusivity. In particular, we will extend the classic steady lee wave energy flux expression of Bell (1975), which has been recently used to estimate lee wave generation in the global ocean (e.g. Nikurashin et al., 2014), to include viscous and diffusive effects. We describe this as the 'viscous lee wave problem'.

Viscous and diabatic internal waves have been investigated theoretically by previous authors, predominantly in the atmospheric context. Pitteway and Hines (1963) examined the decay of waves in upper atmosphere for isotropic viscosity and/or diffusivity. Yanowitch (1967) showed that finite viscosity can act to reflect upward-propagating waves in the atmosphere. These studies considered non-Boussinesq fluids and exponential density profiles appropriate to the atmosphere. Hazel (1967), following Booker and Bretherton (1967), showed that the reflection of waves at critical levels is unchanged by the presence of viscosity, using a similar approach to that taken in the present work of linearising about a background flow state. However, as noted above, here we focus specifically on ocean models with non-isotropic viscosity/diffusivity and apply our results to the lee wave problem.

## 2. Linear wave theory

Here we investigate the dynamics of internal waves generated at a boundary in a 'model fluid' with arbitrary viscosity and/or diffusivity using linear theory. The hydrostatic Boussinesq equations with uniform Laplacian diffusivity (horizontal $\kappa_h$; vertical $\kappa_v$) and viscosity (horizontal $A_h$; vertical $A_v$) on an $f$-plane, linearised about a state with spatially uniform and time-independent background flow, $\mathbf{U} = (U, V, 0)$, and spatially uniform and time-independent stratification, $N^2$, are

$$\frac{\partial u}{\partial t} - fv + \mathbf{U}\cdot\nabla_h u = -\frac{1}{\rho_0}\frac{\partial p}{\partial x} + A_h\nabla_h^2 u + A_v\frac{\partial^2 u}{\partial z^2}, \tag{1a}$$

$$\frac{\partial v}{\partial t} + fu + \mathbf{U}\cdot\nabla_h v = -\frac{1}{\rho_0}\frac{\partial p}{\partial y} + A_h\nabla_h^2 v + A_v\frac{\partial^2 v}{\partial z^2}, \tag{1b}$$

$$0 = -\frac{1}{\rho_0}\frac{\partial p}{\partial z} + b, \tag{1c}$$

$$\frac{\partial b}{\partial t} + wN^2 + \mathbf{U}\cdot\nabla_h b = \kappa_h\nabla_h^2 b + \kappa_v\frac{\partial^2 b}{\partial z^2}, \tag{1d}$$

$$0 = \frac{\partial u}{\partial x} + \frac{\partial v}{\partial y} + \frac{\partial w}{\partial z}, \tag{1e}$$

where $(u, v, w)$ are the velocities in the $(x, y, z)$ Cartesian coordinate directions, $p$ is the pressure, $b = -g(\rho - \rho_0)/\rho_0$ the buoyancy, $f$ the Coriolis parameter, and $\rho_0$ the reference density. We seek solutions to (1) with the form of plane waves moving with the background flow,

$$\begin{aligned} b &= \widehat{b}(k, l, \omega, z)\ \exp\left(\imath(k(x - Ut) + l(y - Vt) + \omega t)\right) \\ &= \widehat{b}(k, l, \Omega, z)\ \exp\left(\imath(kx + ly + \Omega t)\right), \end{aligned} \tag{2}$$

where $\imath = \sqrt{-1}$, $k$, $l$ are the $x$ and $y$ wavenumbers, $\omega$ the Lagrangian frequency, and $\Omega = \omega - (kU + lV)$ the Doppler shifted (Eulerian) frequency. Our objective here is to determine the vertical structure function, $\widehat{b}(k, l, \omega, z)$, which describes the vertical amplitude profile of a wave, given the scale and frequency. Similar expressions to (2) apply for the velocity and pressure fields. Substituting these expressions into (1), and a little manipulation to eliminate the pressure, yields a system of equations,

$$\left(I\frac{\partial^2}{\partial z^2} + A\right)\cdot\mathbf{S} = \mathbf{0}, \tag{3a}$$

where $I$ is the identity matrix,

$$\mathbf{S} = \begin{bmatrix} \widehat{\partial_z u_0} \\ \widehat{\partial_z v_0} \\ \widehat{w}_0 \\ \widehat{b}_0 \end{bmatrix} \tag{3b}$$

and

$$A = \begin{bmatrix} \imath\omega/A_v - K^2A_h/A_v & f/A_v & 0 & -\imath k/A_v \\ -f/A_v & \imath\omega/A_v - K^2A_h/A_v & 0 & -\imath l/A_v \\ \imath k & \imath l & 0 & 0 \\ 0 & 0 & -N^2/\kappa_v & \imath\omega/\kappa_v - K^2\kappa_h/\kappa_v \end{bmatrix} \tag{3c}$$

where $K^2 = k^2 + l^2$. Solutions to the system of Eq. (3) are given by

$$\mathbf{S} = \mathbf{S}(z = 0)\, e^{\gamma z}, \quad (A + \gamma^2 I)\cdot\mathbf{S}(z = 0) = 0, \tag{4}$$

for complex vertical wavenumber $\gamma$ (eigenvalue $\gamma^2$). For non-trivial solutions we must have

$$\begin{aligned} 0 &= \det(A + \gamma^2 I) \\ &= \gamma^2(f^2 + (A_hK^2 - A_v\gamma^2 - \imath\omega)^2)(-K^2\kappa_h + \kappa_v\gamma^2 + \imath\omega) \\ &\quad + K^2\ N^2(A_hK^2 - A_v\gamma^2 - i\omega). \end{aligned} \tag{5}$$

[1] Here, 'smallest possible' refers to the value of explicit viscosity/diffusivity that ensures the flow field is smoothly represented on the model grid at any given location, and therefore depends on both resolution and flow properties. Values smaller than this lead to errors in the numerical advection scheme due to the poor representation of flow gradients (sometimes called 'numerical' diffusion/viscosity) and usually result in the model not being energetically consistent.

Eq. (5) is an fourth order polynomial in $\gamma^2$ and roots may be found numerically in the general case (see below). The four solutions for $\gamma^2$ permit the application of four boundary conditions (on $w$, $b$ and the horizontal shears $\partial_z u$ and $\partial_z v$) at $z = 0$. The square root of $\gamma^2$ is chosen such that $\Re(\gamma) < 0$ and the solutions decay as $z \to \infty$. Three of the four solutions correspond to boundary layers with vertical decay scales of order $h \sim \sqrt{A_v/\omega} = 0.1 - 10\text{m}$ (or $h \sim \sqrt{\kappa_v/\omega}$) for typical values of vertical viscosity, $A_v = 10^{-6} - 10^{-2}$ m$^2$ s$^{-1}$, and $\omega \sim f \sim 10^{-4}$ s$^{-1}$. The presence (or otherwise) of these solutions in a given model depends on the boundary conditions (i.e. boundary fluxes of density and momentum) and is not of interest here (although dissipation from these boundary processes may be globally significant; see Sen et al., 2008). Instead, we focus on the fourth solution, which has an order-of-magnitude larger decay scale, and corresponds to the 'weakly viscous limit' where the equation is soluble analytically. The weakly viscous solutions collapse back to the classical inviscid wave solutions in the limit of zero viscosity, whereas the boundary layer solutions have no inviscid equivalent.

In general $\gamma$ will have real and imaginary parts; let

$$\gamma = \imath m + \frac{1}{h} = \imath m(1 - a\imath) \tag{6}$$

where $m$ is the vertical wavenumber and $h = 1/(am)$ is the decay depth. The quantity $a = 1/(hm) = \lambda/(2\pi h)$ is the fractional (non-dimensional) decay per wavelength $\lambda$. We now introduce appropriately defined Reynolds and Peclet numbers to describe the relative strength of the viscosity and diffusivity:

$$\begin{aligned} \text{Re}_h &= \omega/(A_h K^2), \quad \text{Re}_v = \omega/(A_v m^2), \\ \text{Pe}_h &= \omega/(\kappa_h K^2), \quad \text{Pe}_v = \omega/(\kappa_v m^2). \end{aligned} \tag{7}$$

In terms of these non-dimensional numbers (5) becomes

$$\begin{aligned} 0 = (1 - \imath a)^2 &\left( \left(\frac{f}{\omega}\right)^2 + \left( \frac{1}{\text{Re}_h} + \frac{1}{\text{Re}_v}(1 - \imath a)^2 - \imath \right)^2 \right) \\ &\times \left( \frac{1}{\text{Pe}_h} + \frac{1}{\text{Pe}_v}(1 - \imath a)^2 - \imath \right) \\ &+ \frac{K^2\, N^2}{m^2 \omega^2} \left( \frac{1}{\text{Re}_h} + \frac{1}{\text{Re}_v}(1 - \imath a)^2 - i \right). \end{aligned} \tag{8}$$

The weakly viscous and diffusive solution is the one in which all Re $\gg 1$ and all Pe $\gg 1$. In addition we will assume (to be confirmed below) that the viscosity/diffusivity is sufficiently small that the decay scale is much larger than the wavelength, or $a \ll 1$. Expanding (8) to first order in this limit (i.e. $\text{Re}^{-1} \sim \text{Pe}^{-1} \sim a \ll 1$) yields

$$\begin{aligned} 0 = \imath &\left[ 1 - \frac{K^2\, N^2}{m^2 \omega^2} - \frac{f^2}{\omega^2} \right] \\ &+ \left[ 2a \left( 1 - \frac{f^2}{\omega^2} \right) + \left( \frac{1}{\text{Re}_h} + \frac{1}{\text{Re}_v} \right) \left( \frac{K^2\, N^2}{m^2 \omega^2} - 2 \right) \right. \\ &\left. + \left( \frac{1}{\text{Pe}_h} + \frac{1}{\text{Pe}_v} \right) \left( \frac{f^2}{\omega^2} - 1 \right) \right]. \end{aligned} \tag{9}$$

The expressions for $m$ and $a$ are obtained by setting the real and imaginary parts of (9) to zero. The vertical wavenumber $m$ is

$$m = \frac{NK}{\sqrt{\omega^2 - f^2}}, \tag{10}$$

and the non-dimensional decay rate $a$ is

$$a = \frac{\left(\text{Re}_h^{-1} + \text{Re}_v^{-1}\right)\left(\omega^2 + f^2\right) + \left(\text{Pe}_h^{-1} + \text{Pe}_v^{-1}\right)\left(\omega^2 - f^2\right)}{2(\omega^2 - f^2)}. \tag{11}$$

Eq. (11) implies that our a priori assumption that $a \ll 1$ will hold except where $\omega \to f$. At such near-inertial frequencies the vertical wavelength and decay scale both become small, and the propagating wave solution collapses to a 'boundary layer' solution as discussed above. The decay depth $h$ corresponding to (11) is the geometric mean of the decay depths due to each of the viscous and diffusive terms; dimensionally,

$$\begin{aligned} h^{-1} &= \frac{NK}{2\omega\sqrt{\omega^2 - f^2}} \left( \kappa_v m^2 + \kappa_h K^2 + \frac{\omega^2 + f^2}{\omega^2 - f^2}\left(A_v m^2 + A_h K^2\right) \right) \\ &= \frac{1}{h_{\kappa_v}} + \frac{1}{h_{\kappa_h}} + \frac{1}{h_{A_v}} + \frac{1}{h_{A_h}}, \end{aligned} \tag{12}$$

Note that $h^{-1}$ and $m$ are both imaginary when $\omega < f$, implying $h^{-1}$ becomes the wavenumber and $m$ the decay rate. In the inviscid limit the wavenumber $h^{-1} \to 0$ for $\omega < f$; hence these are often called 'non-wave frequencies'. This clear separation between wave and non-wave frequencies breaks down in the presence of viscosity since all frequencies have a non-zero wavenumber (albeit small for $\omega < f$). Independent of the viscosity or diffusivity, frequencies $\omega < f$ decay rapidly away from the boundary with inviscid decay depth $|m| = NK/\sqrt{f^2 - \omega^2}$.

Fig. 1 displays the wavenumber $m$ and decay rate $h^{-1}$ for (a) molecular viscous parameters and (b) viscous parameters typical of a large-scale model — here we have used the parameter values from the model of Nikurashin et al. (2013) as an example. All four unique solutions for $\gamma$ (obtained from a direct numerical solution to (5)) are shown with the three boundary layer solutions in colour; as anticipated, these solutions have very large decay rates of $\mathcal{O}(0.1\text{–}10)\text{m}^{-1}$ for all frequencies. In addition, these solutions have a smaller decay rate when the viscosity is larger (i.e. in Fig. 1(b) compared with (a)) implying that the boundary layer is wider — this behaviour is opposite to what is expected for propagating waves. The propagating wave solution (defined as the solution with smallest decay rate) determined numerically is shown in black and the analytic solution (from (10) and (12)) in grey — where the numerical solution is not visible (e.g. Fig. 1(a)) it agrees exactly with the analytic, and the black line is beneath the grey. For the weakly viscous solution, the decay rate for 'wave frequencies' $\omega > f$ is increased for larger viscous parameters. For instance, the decay rate at $1.2f$ for molecular values is $10^{-6}$ m$^{-1}$ versus $10^{-2}$ m$^{-1}$ for a typical large-scale model. The decay rate for the 'non-wave frequencies' $\omega < f$ is $NK/\sqrt{f^2 - \omega^2}$, as noted above, independent of the viscosity. The analytic weakly viscous solution is valid everywhere except very close to $f$ (specifically $|\omega - f| < f(\text{Re}_h^{-1} + \text{Re}_v^{-1})/2$) where decay rates are large ($h^{-1} > 10^{-2}\text{m}^{-1}$), and the solution becomes comparable to the other three boundary layer solutions.

Fig. 2 displays the analytic solution for $\omega > f$ split into the separate decay rates due to each of four the vertical and horizontal viscosities and diffusivities. For molecular values, the decay of waves is dominated by the vertical viscosity for frequencies less than about $2f$ and an even contribution from the vertical viscosity and diffusivity for higher frequencies. For very high frequencies where $k > m$ (about $8f$ for the present example), the horizontal terms will dominate, but there is seldom significant energy at such frequencies. In contrast, for the large-scale model values, the decay rate is dominated by the horizontal viscosity for all frequencies and the vertical contribution is entirely negligible (the horizontal diffusivity would also be significant if it was of similar order to the viscosity).

### 2.1. Energy dissipation and fluxes

As noted in the previous section, the clear separation of wave (purely imaginary wavenumber) and non-wave (purely real wavenumber) flow breaks down in the presence of viscosity. How-

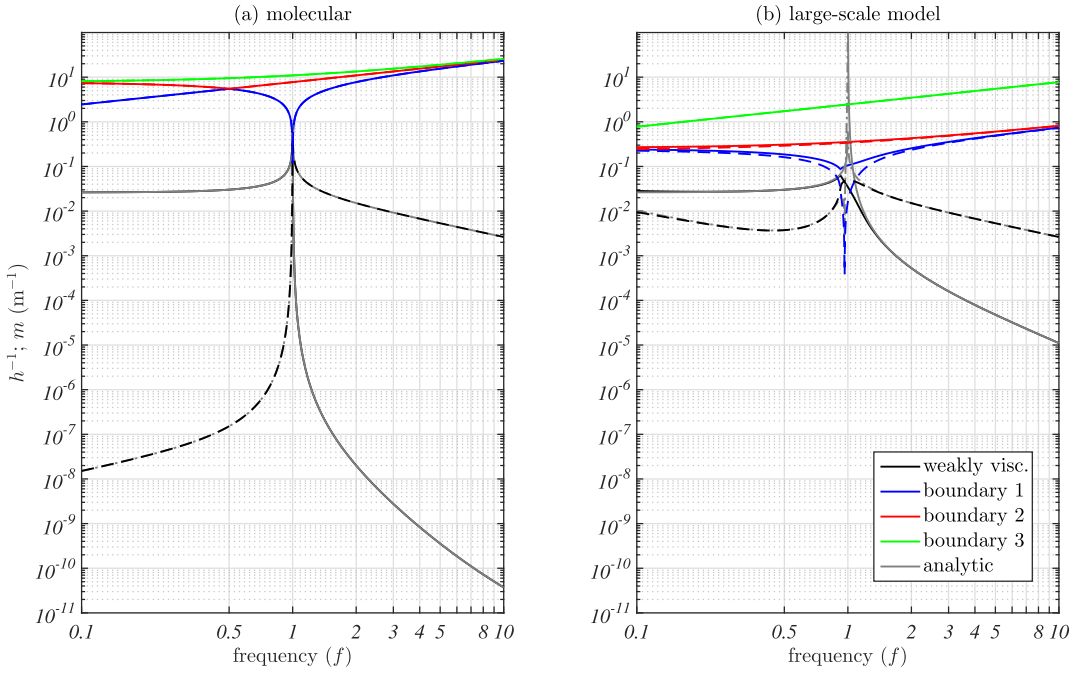


**Fig. 1.** Wavenumbers ($m$, dashed) and decay rates ($h^{-1}$, solid) for a $\lambda = 2$ km wavelength and varying wave frequencies for (a) molecular values of viscosity/diffusivity and (b) typical large-scale model values (e.g. Nikurashin et al., 2013). The four numerical solutions to the eigenvalue Eq. (5) are shown: three of these are 'boundary layer' solutions with large decay rates and are shown in blue, red and green. The fourth 'propagating wave' solution is shown in black. For comparison, the analytic weakly viscous solution is shown in gray and agrees with the numerical wave solution, except near $f$ (where the solutions agree, the black line lies beneath the grey and is not visible). Many of the boundary layer solutions have $m \simeq h^{-1}$ for a significant range of frequencies; in this case the solid and dashed lines are overlaid. Parameters: (a) $A_h = A_v = \kappa_h = \kappa_v = 10^{-6}\text{m}^2\text{s}^{-1}$; (b) $A_h = 1$, $A_v = 10^{-3}$, $\kappa_h = \kappa_v = 10^{-5}\text{m}^2\text{s}^{-1}$.

ever, here we will continue to identify the wave flow as $\omega > f$ for comparison with previous results (e.g. Bell, 1975).

The amount of energy lost by waves at a given vertical level may be computed by forming the energy budget. The equation for the time evolution of kinetic energy, $E_K = (u^2 + v^2)/2$, is obtained by multiplying (1a) by $u$, (1b) by $v$, summing the two equations, and then integrating in $x$ and $y$ to yield

$$\frac{\partial \langle E_K \rangle}{\partial t} = -\frac{1}{\rho_0}\frac{\partial}{\partial z}\langle wp \rangle + \langle wb \rangle - A_h \langle |\nabla_h \mathbf{u}_h|^2 \rangle - A_v \left\langle \left| \frac{\partial \mathbf{u}_h}{\partial z} \right|^2 \right\rangle,$$
$$= -\frac{\partial F}{\partial z} + \langle wb \rangle - \epsilon, \tag{13}$$

where angled brackets $\langle\rangle$ denote the horizontal average, $F = \langle wp \rangle/\rho_0$ is the vertical energy flux, and $\epsilon$ is the total viscous dissipation. Similarly, the equation for the time evolution of available potential energy (APE), $E_A = b^2/(2N^2)$, is obtained by multiplying (1d) by $b$, dividing by $N^2$, and then integrating in $x$ and $y$ to yield

$$\frac{\partial \langle E_A \rangle}{\partial t} = -\langle wb \rangle - \frac{\kappa_h}{N^2}\langle |\nabla_h b|^2 \rangle - \frac{\kappa_v}{N^2}\left\langle \left| \frac{\partial b}{\partial z} \right|^2 \right\rangle,$$
$$= -\langle wb \rangle - \phi_i, \tag{14}$$

where $\phi_i$ is the total irreversible mixing. The total perturbation energy, $E = E_K + E_A$, thus evolves according to

$$\frac{\partial \langle E \rangle}{\partial t} = -\frac{\partial F}{\partial z} - \epsilon - \phi_i,$$
$$= -\frac{\partial F}{\partial z} - D. \tag{15}$$

Thus at steady state the decay of the energy flux $F$ with height corresponds to a deposition of energy ($D = \epsilon + \phi_i$) either via viscous dissipation, $\epsilon$, or irreversible mixing, $\phi_i$. Using Parseval's theorem we can compute this energy deposition as an integral over all wavenumbers and appropriate frequencies,

$$\phi_i = \frac{1}{(2\pi)^3 N^2}\iiint (\kappa_h K^2 + \kappa_v |\gamma|^2)|\widehat{b}_0|^2 e^{-\frac{2|z|}{h}}\, dk\, dl\, d\omega, \tag{16}$$

and

$$\epsilon = \frac{1}{(2\pi)^3}\iiint \left(A_h K^2 + A_v |\gamma|^2\right)\left(|\widehat{u}_0|^2 + |\widehat{v}_0|^2\right) e^{-\frac{2|z|}{h}}\, dk\, dl\, d\omega. \tag{17}$$

Eqs. (16) and (17) are general expressions which we now simplify in the weakly viscous limit. First, we rewrite (17) in terms of the buoyancy. Eq. (3) implies that

$$\gamma\,\widehat{v}_0 + \frac{\omega}{f}\left(\imath - \text{Re}_v^{-1}(1 - \imath a)^2 - \text{Re}_h^{-1}\right)\gamma\,\widehat{u}_0 = \frac{\imath k\,\widehat{b}_0}{f},$$
$$-\gamma\,\widehat{u}_0 + \frac{\omega}{f}\left(\imath - \text{Re}_v^{-1}(1 - \imath a)^2 - \text{Re}_h^{-1}\right)\gamma\,\widehat{v}_0 = \frac{\imath l\,\widehat{b}_0}{f}, \tag{18}$$

in terms of the non-dimensional parameters. Solving (18) in the weakly viscous limit yields

$$\widehat{v}_0 = \frac{1}{\gamma}\frac{\imath k + \frac{\omega}{f}(\imath - \frac{1}{\text{Re}_v} - \frac{1}{\text{Re}_h})\imath l}{1 - \frac{\omega^2}{f^2}}\frac{\widehat{b}_0}{f} + \mathcal{O}(\text{Re}^{-2})$$
$$\widehat{u}_0 = \frac{1}{\gamma}\frac{-\imath l + \frac{\omega}{f}(\imath - \frac{1}{\text{Re}_v} - \frac{1}{\text{Re}_h})\imath k}{1 - \frac{\omega^2}{f^2}}\frac{\widehat{b}_0}{f} + \mathcal{O}(\text{Re}^{-2}). \tag{19}$$

Noting that $|\gamma|^2 = m^2 + h^{-2} = m^2 + \mathcal{O}(\text{Re}^{-2})$, we have

$$|\widehat{u}_0|^2 + |\widehat{v}_0|^2 = \frac{1}{m^2}\frac{K^2(\omega^2 + f^2)}{(\omega^2 - f^2)^2}|\widehat{b}_0|^2 + \mathcal{O}(\text{Re}^{-2}), \tag{20}$$

$$= \frac{1}{N^2}\frac{\omega^2 + f^2}{|\omega^2 - f^2|}|\widehat{b}_0|^2 + \mathcal{O}(\text{Re}^{-2}), \tag{21}$$

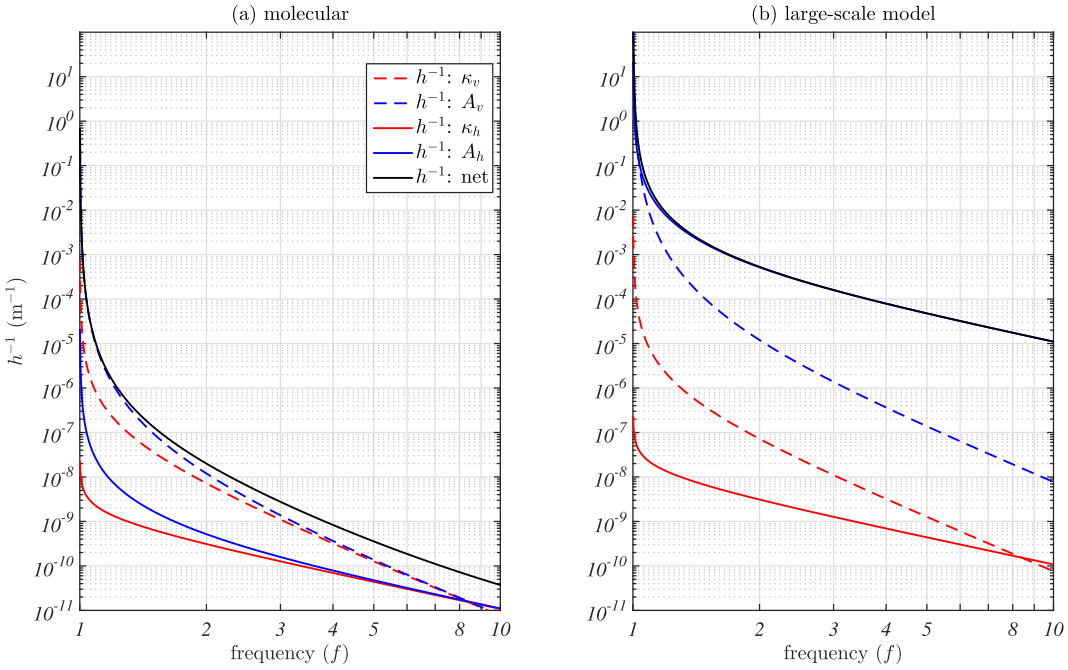


**Fig. 2.** Decay rate of wave amplitude for a $\lambda = 2$ km wavelength and varying wave frequencies for (a) molecular values of viscosity/diffusivity and (b) typical large-scale model values (e.g. Nikurashin et al., 2013). The total decay rate is shown in black, which is comprised of contributions from vertical diffusivity (red-dash), vertical viscosity (blue-dash), horizontal diffusivty (red-solid) and horizontal viscosity (blue-solid). Parameter values are the same as in the previous figure.

and the viscous dissipation (17) may be expressed as

$$\epsilon = \frac{1}{(2\pi)^3 N^2} \iiint \left(A_h K^2 + A_v |m|^2\right) \frac{\omega^2 + f^2}{|\omega^2 - f^2|} |\widehat{b}_0|^2 e^{-\frac{2|z|}{h}} \, dk \, dl \, d\omega, \tag{22}$$

in the weakly viscous limit. The corresponding irreversible mixing (16) in the weakly viscous limit is

$$\phi_i = \frac{1}{(2\pi)^3 N^2} \iiint \left(\kappa_h K^2 + \kappa_v |m|^2\right) |\widehat{b}_0|^2 e^{-\frac{2|z|}{h}} \, dk \, dl \, d\omega. \tag{23}$$

The net energy deposition, $D = \epsilon + \phi_i$, from the wave flow (i.e. integral over $\omega > f$) is thus

$$D_w = \frac{1}{(2\pi)^3} \int_f^\infty \iint \frac{2\omega\sqrt{\omega^2 - f^2}}{N^3 K h} e^{-\frac{2|z|}{h}} |\widehat{b}_0(k, l, \omega)|^2 \, dk \, dl \, d\omega, \tag{24}$$

where $h$ is the viscous/diffusive wave decay depth from (12). The wave energy flux at a given depth, $F_w = |wp|/\rho_0$, can now be computed as the vertical integral (e.g. (15)) of the net energy deposition defined by (24),

$$F_w(z) = \frac{1}{(2\pi)^3} \int_f^\infty \iint \frac{\omega\sqrt{\omega^2 - f^2}}{N^3 K} \, e^{-\frac{2|z|}{h}} |\widehat{b}_0(k, l, \omega)|^2 \, dk \, dl \, d\omega. \tag{25}$$

The above results can describe many different mechanisms of wave forcing at boundaries through an appropriate choice of $\widehat{b}_0(k, l, \omega)$. We consider the particular case of steady lee waves in the next section.

### 2.2. Steady lee waves

Lee waves are generated by large-scale flow over topography in a stratified fluid. The linearised boundary condition is that flow is parallel to the topography, or $w = \mathbf{U}_h \cdot \nabla_h H$, where $H(x, y)$ is the height of the bottom topography above $z = 0$. For small amplitude topography, the boundary condition is applied at $z = 0$ and thus $\widehat{w}_0 = (-\imath k U - \imath l V)\widehat{H}$, or in terms of buoyancy (from (3))

$$\widehat{b}_0(k, l, \omega) = \frac{N^2 \widehat{w}_0}{\imath\omega - \kappa_h K^2 + \kappa_v \gamma^2}. \tag{26}$$

Assuming that the fluid is weakly diffusive (Pe $\gg 1$), as previously, (26) simplifies to

$$\widehat{b}_0(k, l, \omega) = \frac{-N^2 \widehat{H}\,(kU + lV)}{\omega}, \tag{27}$$

For *steady* lee waves we require the Eulerian frequency $\Omega = \omega - (kU + lV) = 0$, and thus the Lagrangian frequency is $\omega = (kU + lV)$ and (27) becomes

$$\widehat{b}_0(k, l, \omega) = -N^2 \widehat{H}\, 2\pi\, \delta(\omega - (kU + lV)), \tag{28}$$

where $\delta$ is the Dirac delta function. Substituting (28) into (25) and, without loss of generality, choosing our $x$-axis to coincide with the local flow, the lee wave energy flux is

$$F_w = \frac{1}{(2\pi)^2} \iint_{f/U}^\infty NU \frac{k}{K} \sqrt{k^2U^2 - f^2} e^{-\frac{2z}{h}} |\widehat{H}|^2 \, dk \, dl, \tag{29}$$

where

$$h = \frac{2kU\sqrt{k^2U^2 - f^2}}{NK} \times \left( (K^2\kappa_h + m^2\kappa_v) + \frac{k^2U^2 + f^2}{k^2U^2 - f^2} (K^2 A_h + m^2 A_v) \right)^{-1}, \tag{30}$$

and

$$m = \frac{NK}{\sqrt{k^2U^2 - f^2}}. \tag{31}$$

Eq. (29) agrees with the usual expression (e.g. Bell, 1975) for the hydrostatic steady lee wave energy flux at $z = 0$, but unlike the classical inviscid/adiabatic problem, the flux decays with height over $e$-folding scale $h/2$.

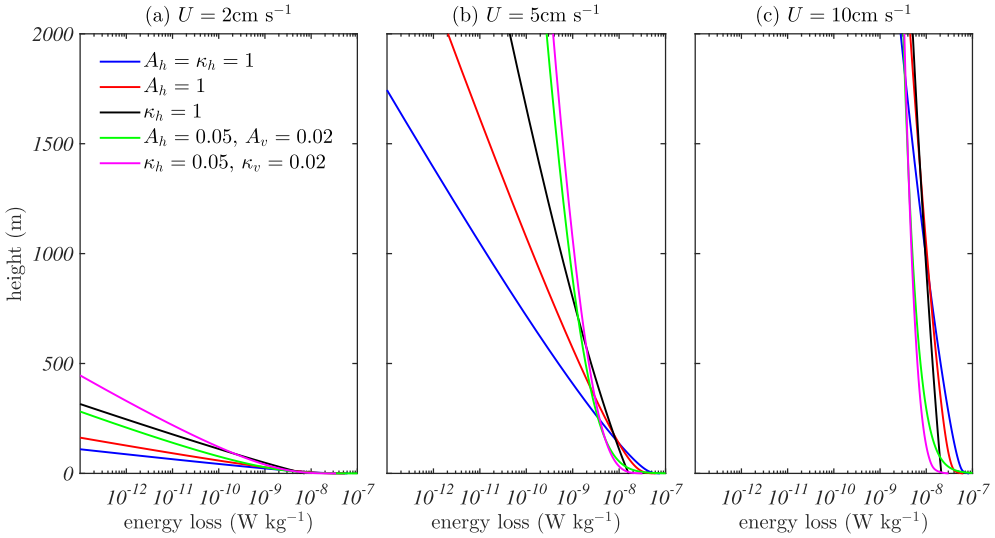


**Fig. 3.** The total energy loss from the wave flow for five choices of viscous parameters (see legend; units m$^2$ s$^{-1}$, values not specified are zero) and three free-stream speeds: (a) 2 cm s$^{-1}$, (b) 5 cm s$^{-1}$ and (c) 10 cm s$^{-1}$. The topographic spectrum is defined by (32) with the free parameters chosen as described in the text. The buoyancy frequency is taken as $N^2 = 10^{-6}$ s$^{-2}$ and the Coriolis parameter as $f = -1.2 \times 10^{-4}$ s$^{-1}$.

### 2.3. Implications for modelling

To understand the implications of the above results for ocean modelling we need to make appropriate choices for free-stream speed $U$, stratification $N^2$, Coriolis frequency $f$ and the topographic height spectrum $|\widehat{H}|^2$. Here we will use parameters characteristic of the Drake Passage region of the Southern Ocean: $N^2 = 10^{-6}$ s$^{-2}$ and $f = -1.2 \times 10^{-4}$ s$^{-1}$. Goff and Jordan (1988) show that the height spectrum of sea floor topography may be well approximated by

$$|\widehat{H}(k,l)|^2 = \frac{2\pi H_{rms}^2(\mu-2)}{k_0 l_0} \times \left[1 + \frac{K^2}{k_0^2}\cos^2(\phi-\phi_0) + \frac{K^2}{l_0^2}\sin^2(\phi-\phi_0)\right]^{-\mu/2}, \tag{32}$$

where $k_0$ and $l_0$ are the characteristic easterly and northerly wavenumbers, $\phi$ is the angle of the wavevector with respect to east, $H_{rms}$ is the root-mean-square topographic height, $\phi_0$ is the azimuthal angle and $\mu$ characterises the roll-off of the spectrum at high wavenumbers. Here we will use the same parameter values as Nikurashin and Ferrari (2010): $H_{rms} = 305$ m, $\mu = 3.5$, $k_0 = 2.3 \times 10^{-4}$ m$^{-1}$, $l_0 = 1.3 \times 10^{-4}$ m$^{-1}$ and $\phi_0 = 320°$.

Fig. 3 displays the net wave energy deposition $D_w$ from the wave flow given the above parameter choices, for three different free-stream speeds: (a) 2 cm s$^{-1}$, (b) 5 cm s$^{-1}$ and (c) 10 cm s$^{-1}$. The corresponding wave energy flux for each case is shown in Fig. 4. Each plot displays the result for five different sets of viscous parameters; the first three are dominated by horizontal viscosity/diffusivity, and the latter two by vertical. We consider the horizontal first.

#### 2.3.1. Large-scale models: horizontal viscosity

The first three curves in Figs. 3 and 4 involve purely horizontal viscosity and diffusivity ($A_h = \kappa_h = 1$ m$^2$ s$^{-1}$; blue), horizontal viscosity only ($A_h = 1$ m$^2$ s$^{-1}$; red) and horizontal diffusivity only ($\kappa_h = 1$ m$^2$ s$^{-1}$; black). Both the magnitude and decay depth of the energy flux increases with free stream speed as wave generation occurs at larger scales (and higher frequencies). For $U = 2$ cm s$^{-1}$ the (small) wave energy flux (0.2 mW m$^{-2}$) decays within 100 m of the boundary. For $U = 5$ cm s$^{-1}$ the wave energy flux (4.3 mW m$^{-2}$) decays within 1500 m of the boundary. For $U = 10$ cm s$^{-1}$ the wave energy flux (33 mW m$^{-2}$) remains non-zero even at 4 km above the boundary. As a consequence there is significant energy deposition at large distances from the wave source — for example, energy deposition at 4 km height exceeds $10^{-9}$ W kg$^{-1}$. The decay rate of the wave energy flux is significantly less for diffusivity (black curves) compared with viscosity (red curves) of the same magnitude.

We now compare our solutions to the results of recent modelling studies, in particular Nikurashin et al. (2013) who use comparable parameter values ($A_h = 1$ m$^2$ s$^{-1}$ and $\kappa_h \simeq 0$; red curves in Figs. 3 and 4)[2]. The dissipation seen in that study (e.g. Fig. 5(a) therein) is strongly enhanced near the bottom topography, $\mathcal{O}(10^{-8})$ W kg$^{-1}$, and decays rapidly to less than $10^{-9}$ W kg$^{-1}$ within a few hundred metres of the topography, with a net vertically integrated dissipation of 6.1 mW m$^{-2}$ (see their Fig. 2(a)). The enhanced dissipation directly above the topography is likely to be associated with non-wave flow (e.g. Sen et al., 2008) and 'boundary layer' wave solutions of the sort discussed in Section 2 — therefore, the dissipation associated with propagating waves will be less than the quoted 6.1 mW m$^{-2}$. Thus a flow speed of 5 cm s$^{-1}$ (Figs. 3(b) and 4(b)), which corresponds to a net wave energy flux of 4.3 mW m$^{-2}$, seems to be reasonably representative of the numerical model. Fig. 4(b) indicates that the wave energy flux for this flow speed reduces by over 80% within 250 m of the boundary, comparable to the reported numerical model results. Only in regions of particularly strong bottom flow (e.g. 10 cm s$^{-1}$; Fig. 4(c)) are the waves able to transport significant energy outside of the bottom boundary region.

#### 2.3.2. Idealised models: Vertical viscosity

To quantify the effect of vertical viscosity/diffusivity, Figs. 3 and 4 displays the energy deposition and flux for parameter values used in a recent idealised small-scale wave modelling study (e.g. Nikurashin et al., 2014, use $A_h = 0.05$, $A_v = 0.02$, $\kappa_h = \kappa_v =$

[2] Specifically, Nikurashin et al. (2013) use $A_h = 1$ m$^2$ s$^{-1}$, $A_v = 10^{-3}$ m$^2$ s$^{-1}$ and $\kappa_h = \kappa_v = 10^{-5}$ m$^2$ s$^{-1}$, but as shown in Fig. 1(d), only the horizontal viscosity is significant.

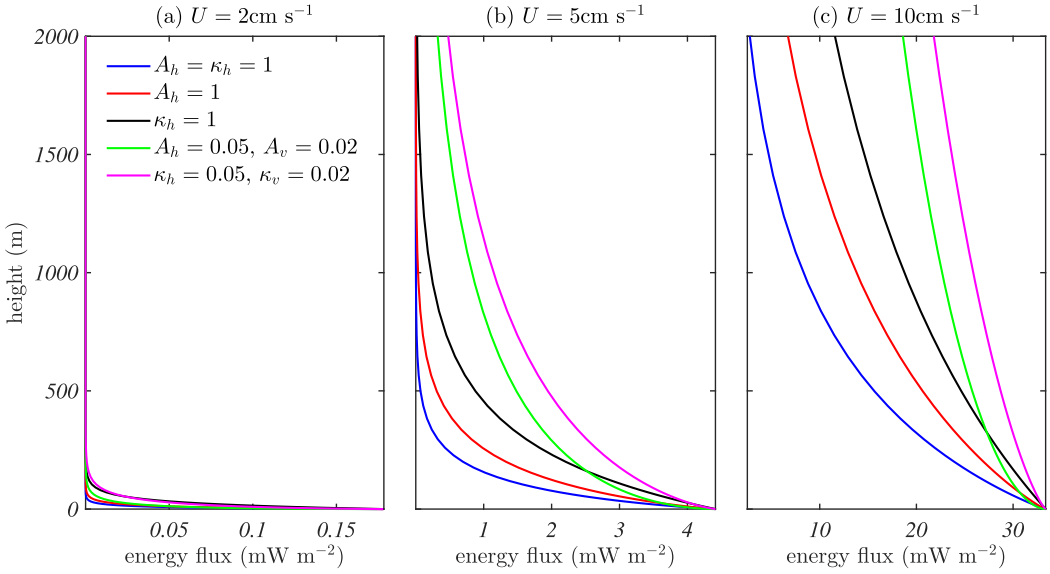


**Fig. 4.** The wave energy flux for six choices of diffusivity/viscosity (see legend; units m$^2$ s$^{-1}$, values not specified are zero) and three free-stream speeds: (a) 2 cm s$^{-1}$, (b) 5 cm s$^{-1}$ and (c) 10 cm s$^{-1}$. Parameter values and topographic spectrum are the same as for the previous figure.

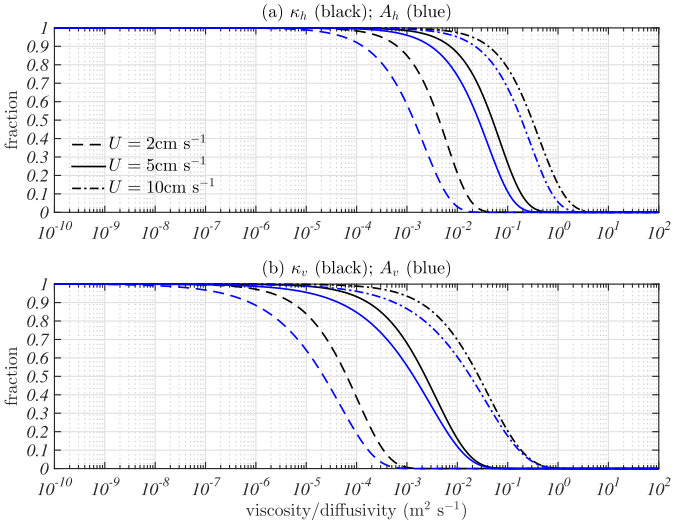


**Fig. 5.** The fraction of the initial steady lee wave energy flux remaining at a vertical height of 4 km above the bottom as a function of (a) horizontal diffusivity (black) or viscosity (blue), and (b) vertical diffusivity (black) or viscosity (blue), for three free-stream speeds $U$ (see legend). Parameter values and topographic spectrum are the same as for the previous figures.

$10^{-5}$ m$^2$ s$^{-1}$; in green). Nikurashin et al. (2014) examine wave generation associated with an imposed background flow of 10 cm s$^{-1}$ in an idealised 10 km square, 2 km deep domain at 40 m horizontal and 10 m vertical resolution. Since the horizontal and vertical viscous parameters are the same order of magnitude, it is the vertical that dominates the dissipation ($A_v m^2 \gg A_h k^2$). Even at this high resolution, the wave energy flux decays by 44% over the 2 km domain depth for the 10 cm s$^{-1}$ background flow (Fig. 4(c)). This rapid decay indicates that the lee wave processes in the Nikurashin et al. (2014) model cannot be regarded as inviscid, contrary to the claims made in that paper. However, we note that the linear decay of the generated waves is unlikely to significantly alter the main results of Nikurashin et al. (2014) since they evaluate the energy flux directly above the topography, and don't compute the dissipation.

Figs. 4 also displays the energy flux if the values for viscosity and diffusivity used by Nikurashin et al. (2014) are switched (in pink; $\kappa_h = 0.05$, $\kappa_v = 0.02$, $A_h = A_v = 10^{-5}$ m$^2$ s$^{-1}$). Similar to the previous section, the diffusivity leads to reduced wave decay compared with viscosity (i.e. the energy flux is 20% larger at 2 km height).

### 2.4. Target parameters

The solutions presented herein provide design criteria for future wave-resolving numerical models. In most models artificially high horizontal viscosity and/or diffusivity is required to prevent the collapse of flow structures below the gridscale. Since diffusivity modifies the wave energy flux less than the viscosity, our first suggestion is that models focusing on wave dynamics use elevated diffusivity rather than viscosity. Diffusivity and viscosity have the same effect in terms of stabilising large-scale geostrophic flow, since one arrests the collapse of density gradients and the other the collapse of velocity gradients, with the velocity and density linked through geostrophy[3].

Further, the viscous lee wave theory developed here may be used to determine the maximum magnitude of diffusivity/viscosity permitted to limit the decay of the wave energy flux in an ocean model to a certain satisfactory level. Fig. 5 shows the fraction of steady lee wave energy flux remaining at the 'ocean surface' (4 km height) as a function of (a) horizontal and (b) vertical diffusivity/viscosity for three flow speeds and the Southern Ocean topography/stratification described in Section 2. The most significant lee wave generation typically occurs for speeds exceeding 5 cm s$^{-1}$. Suppose we require less than 10% linear wave decay at this speed over the ocean depth: the required parameter values would be $\kappa_h < 8 \times 10^{-3}$ or $A_h < 3 \times 10^{-3}$ m$^2$ s$^{-1}$ in the horizontal and $\kappa_v < 2 \times 10^{-4}$ or $A_v < 5 \times 10^{-5}$ m$^2$ s$^{-1}$ in the vertical. The vertical values are comparable to those already used

[3] Using diffusivity in place of viscosity is only likely to be an issue for models focusing on water mass transformation processes where the control of mixing is important. However, such models are typically not wave resolving.

in many regional ocean models. However, current wave-resolving models (e.g. Nikurashin et al., 2013) at $\mathcal{O}(100)$ m resolution require $\mathcal{O}(1)$ m$^2$ s$^{-1}$ horizontal viscosity/diffusivity to ensure that flow gradients are well-resolved and there are no significant errors in the numerical advection scheme (such that the model is energetically consistent). Thus, assuming diffusive/viscous parameters scale with resolution, achieving $\mathcal{O}(0.01)$ m$^2$ s$^{-1}$ horizontal diffusivity *throughout the ocean depth* seems impractical for regional ocean models since it is likely to require $\mathcal{O}(1)$ m horizontal model resolutions. An alternative model design (e.g. Shakespeare and Hogg, 2017) that reduces, but does not eliminate, viscous wave decay is to have elevated diffusivity near the model boundaries (where balanced flow gradients tend to collapse towards the grid-scale), but a near-inviscid and adiabatic interior where waves can propagate freely.

## 3. Discussion

Here we have described the energetics of linear waves in a fluid with elevated values of viscosity and/or diffusivity as is typical of high-resolution numerical ocean models. In particular, we have presented extended solutions to the classical steady lee wave problem (Bell, 1975) that describe the magnitude of energy deposition and decay of the wave energy flux due to elevated viscosity and/or diffusivity. These solutions have important consequences for the modelling of internal waves.

Firstly, our solutions help to interpret recent numerical model results. Ocean observations clearly show enhanced viscous dissipation near the ocean surface and near the ocean bottom, with the bottom dissipation strongly enhanced in regions of rough topography (Waterhouse et al., 2014). This dissipation is thought to be associated with intense diapycnal mixing and hence these regions are important to sustaining the ocean overturning circulation (Wunsch and Ferrari, 2004). Recent wave-resolving model results (Nikurashin et al., 2013) have been interpreted as suggesting this enhanced dissipation is the direct result of locally generated lee waves. However, here we have shown that the dissipation local to rough topography in such wave-resolving models is likely to be a direct result of the subgrid parameterisation (elevated horizontal viscosity and/or diffusivity) used in those models. In some regions of the ocean — for example, ocean boundaries — $\mathcal{O}(1)$ m$^2$ s$^{-1}$ magnitude viscosity/diffusivity could potentially be justified on the basis of parameterising unresolved ($< 200$ m) waves and turbulent motions; however, such values are probably not justified throughout the ocean interior. Furthermore, even if parameterized mixing of density or momentum can be justified with the above magnitude, it is not clear that it should have the form of a Laplacian (or indeed biharmonic) operator. It is questionable whether smaller scale unresolved waves or other motions would act to damp resolved waves in the manner shown here. In the absence of such evidence, we suggest that the dissipation of propagating waves local to rough topography in current wave-resolving models should be regarded as spurious. Indeed, this argument is supported by recent observational studies (Waterman et al., 2013) which report that dissipation near topography is only 2–20% of the theoretical lee wave energy flux. Thus, caution should be exercised in attempting to infer the location and magnitude of wave dissipation from the present generation of high-resolution models.

Secondly, in Section 2.4 we showed that our solutions can be used to aid in the design of future wave-resolving numerical models. We suggest that horizontal viscosity and diffusivity should be limited to less than $10^{-2}$ m$^2$ s$^{-1}$ where possible in order to limit the viscous decay of waves. Similarly, vertical viscosity and diffusivity should be less than $10^{-4}$ m$^2$ s$^{-1}$.

## 4. Conclusions

Internal waves play an important role in the ocean energy budget, and resolving their effect in regional ocean models is a laudable objective. However, the viscous lee wave theory outlined here indicates that careful consideration is required before we can infer dissipation and mixing from such models.

## Acknowledgments

The authors acknowledge funding from the ARC Centre of Excellence for Climate System Science grant number CE1101028. The authors acknowledge the two anonymous reviewers whose comments greatly improved the manuscript.

## References

Alford, M.H., MacKinnon, J.A., Simmons, H.L., Nash, J.D., 2016. Near-inertial internal gravity waves in the ocean. Annu. Rev. Marine Sci. 8, 95–123.
Bell, T., 1975. Topographically generated internal waves in the open ocean. J. Geophys. Res. 80, 320–327.
Booker, J.R., Bretherton, F.P., 1967. The critical layer for internal gravity waves in a shear flow. J. Fluid Mech. 27, 513–539.
Danioux, E., Vanneste, J., Klein, P., Sasaki, H., 2012. Spontaneous inertia-gravity-wave generation by surface-intensifed turbulence. J. Fluid Mech. 699, 153–1732.
Goff, J.A., Jordan, T.H., 1988. Stochastic modeling of seafloor morphology: inversion of sea beam data for second-order statistics. J. Geophys. Res. 93, 13589–13608.
Hazel, P., 1967. The effect of viscosity and heat conduction on internal gravity waves at a critical level. J. Fluid Mech. 30, 775–783.
Jouanno, J., Capet, X., Madec, G., Roullet, G., Klein, P., 2016. Dissipation of the energy imparted by mid-latitude storms in the southern ocean. Ocean Sci. 12, 743–769.
Nagai, T., Tandon, A., Kunze, E., Mahadevan, A., 2015. Spontaneous generation of near-inertial waves by the Kuroshio front. J. Phys. Oceanogr. 45, 2381–2406.
Nikurashin, M., Ferrari, R., 2010. Radiation and dissipation of internal waves generated by geostrophic motions impinging on small-scale topography: theory. J. Phys. Oceanogr. 40, 1055–1074.
Nikurashin, M., Ferrari, R., Grisouard, N., Polzin, K., 2014. The impact of finite-amplitude bottom topography on internal wave generation in the southern ocean. J. Phys. Oceanogr. 44, 2938–2950.
Nikurashin, M., Vallis, G.K., Adcroft, A., 2013. Routes to energy dissipation for geostrophic flows in the southern ocean. Nature Geosci. 6, 48–51.
Pitteway, M., Hines, C., 1963. The viscous damping of atmospheric gravity waves. Can. J. Phys 41, 1935–1948.
Polzin, K.L., 2010. Mesoscale eddy-internal wave coupling. part II: energetics and results from polymode. J. Phys. Oceanogr. 40, 789–801.
Polzin, K.L., Lvov, Y.V., 2011. Toward regional characterizations of the oceanic internal wavefield. Rev. Geophys. 49.
Rosso, I., Hogg, A.M., Kiss, A.E., Gayen, B., 2015. Topographic influence on submesoscale dynamics in the southern ocean. Geophys. Res. Lett. 42, 1139–1147. doi:10.1002/2014GL062720.
Sen, A., Scott, R.B., Arbic, B.K., 2008. Global energy dissipation rate of deep-ocean low-frequency flows by quadratic bottom boundary layer drag: computations from current-meter data. Geophys. Res. Lett. 35.
Shakespeare, C.J., Hogg, A.M., 2017. Spontaneous surface generation and interior amplification of internal waves in a regional-scale ocean model. J. Phys. Oceanogr. doi:10.1175/JPO-D-16-0188.1.
Shakespeare, C.J., Taylor, J.R., 2016. Spontaneous wave generation at strongly strained density fronts. J. Phys. Oceanogr. 2063–2081. doi:10.1175/jpo-d-15-0043.1.
St Laurent, L., Garrett, C., 2002. The role of internal tides in mixing the deep ocean. J. Phys. Oceanogr. 32, 2882–2899.
Vanneste, J., 2013. Balance and spontaneous wave generation in geophysical flows. Annu. Rev. Fluid Mech. 45, 147–172.
Waterhouse, A.F., MacKinnon, J.A., Nash, J.D., Alford, M.H., Kunze, E., Simmons, H.L., Polzin, K.L., St. Laurent, L.C., Sun, O.M., Pinkel, R., et al., 2014. Global patterns of diapycnal mixing from measurements of the turbulent dissipation rate. J. Phys. Oceanogr. 44, 1854–1872.
Waterman, S., Naveira Garabato, A.C., Polzin, K.L., 2013. Internal waves and turbulence in the antarctic circumpolar current. J. Phys. Oceanogr. 43, 259–282.
Wunsch, C., Ferrari, R., 2004. Vertical mixing, energy and the general circulation of the oceans. Annu. Rev. Fluid Mech. 36, 281–314.
Yanowitch, M., 1967. Effect of viscosity on gravity waves and the upper boundary condition. J. Fluid Mech. 29, 209–231.